

Note: This is a draft of a paper submitted for publication. Contents of this paper should not be quoted or referred to without permission of the author(s).

## **Ion-Beam-Induced Defects and Defect Interactions in Perovskite-Structure Titanates**

W. J. Weber, W. Jiang, S. Thevuthasan, and R. E. Williford  
Pacific Northwest National Laboratory, Richland, Washington 99352

A. Meldrum and L. A. Boatner  
Solid State Division, Oak Ridge National Laboratory, Oak Ridge, TN 37831

Submitted to  
*NATO Advanced Research Workshop on "Defects and Surface-Induced Effects in  
Advanced Perovskites"*  
*Jurmala, Latvia*  
*August 23-25, 1999*

"The submitted manuscript has been authored by a contractor of the U.S. Government under contract No. DE-AC05-96OR22464. Accordingly, the U.S. Government retains a nonexclusive, royalty-free license to publish or reproduce the published form of this contribution, or allow others to do so, for U.S. Government purposes."

prepared by  
SOLID STATE DIVISION  
OAK RIDGE NATIONAL LABORATORY  
Managed by  
LOCKHEED MARTIN ENERGY RESEARCH CORP.  
under  
Contract No. DE-AC05-96OR22464  
with the  
U.S. DEPARTMENT OF ENERGY  
Oak Ridge, Tennessee

August 1999

## ION-BEAM-INDUCED DEFECTS AND DEFECT INTERACTIONS IN PEROVSKITE-STRUCTURE TITANATES

W.J. WEBER, W. JIANG, S. THEVUTHASAN, and R.E. WILLIFORD  
*Pacific Northwest National Laboratory*  
*Richland, Washington 99352, USA*

A. MELDRUM and L.A. BOATNER  
*Oak Ridge National Laboratory*  
*Oak Ridge, Tennessee 37831, USA*

### Abstract

Ion-beam irradiation of perovskite structures results in the production and accumulation of defects. Below a critical temperature, irradiation also leads to a crystalline-to-amorphous transformation. The critical temperature for amorphization under 800 keV  $\text{Kr}^+$  ion irradiation is 425, 440 and 550 K for  $\text{SrTiO}_3$ ,  $\text{CaTiO}_3$  and  $\text{BaTiO}_3$ , respectively. The results of ion-channeling studies on  $\text{SrTiO}_3$  irradiated with 1.0 MeV  $\text{Au}^{2+}$  ions suggest that the crystalline-to-amorphous transformation is dominated by the accumulation and interaction of irradiation-induced defects. In  $\text{SrTiO}_3$  irradiated with  $\text{He}^+$  and  $\text{O}^+$  ions at 180 K, isochronal annealing studies indicate that there is significant recovery of defects on both the oxygen and cation sublattices between 200 and 400 K. These results suggest that defect recovery processes may control the kinetics of amorphization. A fit of the direct-impact/defect-stimulated model to the data for  $\text{SrTiO}_3$  suggests that the kinetics of amorphization are controlled by both a nearly athermal irradiation-assisted recovery process with an activation energy of  $0.1 \pm 0.05$  eV and a thermal defect recovery process with an activation energy of  $0.6 \pm 0.1$  eV. In  $\text{SrTiO}_3$  implanted with 40 keV  $\text{H}^+$  to  $5.0 \times 10^{16}$  and  $1.0 \times 10^{17}$  ions/cm<sup>2</sup>, annealing at 470 K increases the backscattering yield from Sr and Ti and is mostly likely due to the coalescence of  $\text{H}_2$  into bubble nuclei. Annealing at 570 K and higher results in the formation of blisters or large cleaved areas.

### 1. Introduction

Compounds with the perovskite structure represent a rich class of materials with potential applications ranging from electronic and optoelectronic devices to the immobilization of nuclear wastes. Irradiation with energetic ions can be used to modify the surface and near-surface properties of such materials, introduce new elements and defects, induce phase transformations, and study irradiation effects. Subsequent thermal annealing can lead to full or partial recovery, evolution of new microstructures, and the

determination of activation energies associated with various recovery stages. Consequently, irradiation with energetic ions and subsequent thermal annealing can be used to induce and study a rich set of defects and transformation processes in perovskite structures that could lead to technological advances.

Many oxides with the perovskite structure undergo an irradiation-induced crystalline-to-amorphous phase transition [1-10]; however, the mechanism for this irradiation-induced amorphization has not yet been identified. In several of these studies, thermal annealing was utilized to study the epitaxial regrowth of the ion-beam-induced amorphized layers [1-6,8]. The activation energies for epitaxial regrowth have been determined to be 0.95 and 1.85 eV for  $\text{SrTiO}_3$  [4] and  $\text{CaTiO}_3$  [8], respectively, in moist ( $\text{H}_2\text{O}$ ) atmospheres. In dry atmospheres, the activation energies for epitaxial regrowth have been determined to increase to 1.2 and 3.9 eV for  $\text{SrTiO}_3$  [4] and  $\text{CaTiO}_3$  [8], respectively. Several perovskite-structure oxides also undergo one or more displacive phase transitions at temperatures below the critical temperature for amorphization; however, no significant effects of this transition on amorphization have been observed [9].

In the present study, the results for ion-beam-induced disordering in  $\text{CaTiO}_3$ ,  $\text{SrTiO}_3$ , and  $\text{BaTiO}_3$  are reviewed, and new results are presented. In addition, the results from thermal annealing of ion-beam-induced damage in  $\text{SrTiO}_3$  are reported. Some of these results have been reported previously [9-11].

## 2. Experimental procedures

As described previously [9], the single crystals of  $\text{CaTiO}_3$  and  $\text{BaTiO}_3$  used in the studies conducted by Oak Ridge National Laboratory (ORNL) were grown by a flux technique, while the  $\text{SrTiO}_3$  single crystals were grown by flame fusion. Specimens for transmission electron microscopy (TEM) were prepared by hand polishing and then ion milling at 77 K with 4 keV  $\text{Ar}^+$  ions. The specimens were irradiated at the HVEM-Tandem facility (i.e., in vacuum) at Argonne National Laboratory (ANL) using either 0.8 MeV  $\text{Kr}^+$  or 0.8 MeV  $\text{Xe}^+$  at an ion flux of  $1.7 \times 10^{12}$  ions/ $\text{cm}^2/\text{s}$ . The irradiation-induced amorphization was monitored *in situ*, using electron diffraction techniques, as a function of temperature. To facilitate comparisons of dose dependence, the ion fluence for complete amorphization was normalized to an equivalent displacement dose in displacements per atom (dpa) using TRIM 97 and a displacement energy of 25 eV.

The  $\text{SrTiO}_3$  single crystals used in the studies at the Pacific Northwest National Laboratory (PNNL) were obtained from Commercial Crystal Laboratories, Inc. and were oriented along the [100] axis. Both the accumulation of disorder and subsequent thermal recovery were followed *in situ* using 2 MeV  $\text{He}^+$  Rutherford Backscattering Spectroscopy in channeling geometry (RBS/C), as described previously [10]. The single crystals were irradiated at 180 to 200 K with 410 keV  $\text{He}^+$ , 400 keV  $\text{O}^+$  or 1.0 MeV  $\text{Au}^{2+}$  ions at an incident angle of  $60^\circ$ , which produced near-surface damage that could be probed by RBS/C methods. The irradiation and *in situ* ion-beam analysis were carried out using the accelerator facility at the Environmental Molecular Sciences Laboratory at PNNL. Single crystals of  $\text{SrTiO}_3$  were also implanted at 120 K with 40 keV  $\text{H}^+$  ions by Implant Sciences Corporation to ion fluences of  $5.0 \times 10^{16}$  and  $1.0 \times$

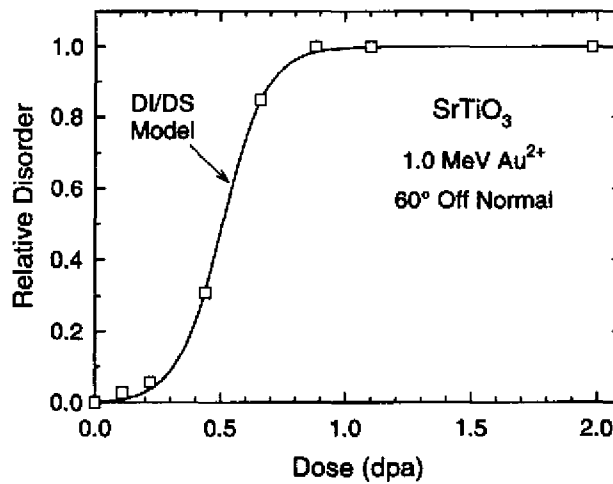


Figure 1. Relative disorder at the damage peak in  $\text{SrTiO}_3$  irradiated at 200 K with 1.0 MeV  $\text{Au}^{2+}$  ions. Also shown is a fit of Eq. (1) to the data.

$10^{17}$  ions/cm<sup>2</sup> [11]. These hydrogen-implanted samples were subsequently characterized and subjected to a thermal annealing study at PNNL. Isochronal annealing on all these samples was performed *in situ* (i.e., in vacuum) at temperatures ranging from 300 to 870 K for time periods of 20 minutes. After each annealing step, the sample was cooled down, and the RBS/C measurements were performed at 300 K. In the case of the hydrogen-implanted samples, hydrogen nuclear reaction analysis (NRA) was also carried out, using the resonant  $^1\text{H}(^{19}\text{F}, \alpha)^{16}\text{O}$  reaction, to monitor the hydrogen profile. The sample was in random orientation during the hydrogen profile measurements, and Mylar film was used for hydrogen calibration.

### 3. Results and discussions

#### 3.1. DAMAGE ACCUMULATION

The accumulation of relative disorder as a function of dose (dpa) in  $\text{SrTiO}_3$  irradiated at 200 K with 1.0 MeV  $\text{Au}^{2+}$  ions is shown in Figure 1. The relative disorder shows a very strong sigmoidal dependence on dose, and the results indicate that the random level (or amorphous state) is reached at a dose of about 1.0 dpa. As discussed elsewhere [12], several models of amorphization can be used to describe the sigmoidal behavior shown in Figure 1. One model that has proven useful is the direct-impact/defect-stimulated (DI/DS) model for amorphization [12]. In the absence of any recovery processes, the amorphous fraction,  $f_a$ , in this model is given by the following expression:

$$f_a = 1 - (\sigma_a + \sigma_s) / \{\sigma_s + \sigma_a \exp[(\sigma_a + \sigma_s)D]\}, \quad (1)$$

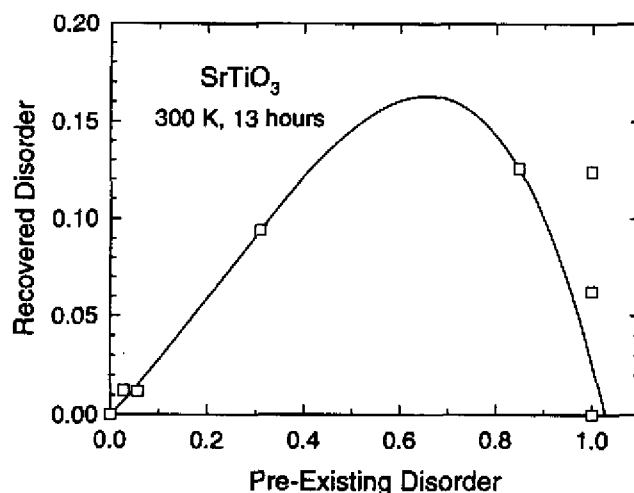


Figure 2. Recovery of disorder at 300 K (13 hours) as a function of pre-existing disorder in  $\text{SrTiO}_3$  irradiated at 200 K with 1.0 MeV  $\text{Au}^{2+}$  ions.

where  $\sigma_d$  and  $\sigma_i$  are effective cross sections for direct-impact and defect-stimulated amorphization, respectively, and  $D$  is the dose. A fit of this model to the data is shown in Figure 1 and yields a value of about 300 for  $\sigma_i/\sigma_d$ , which is the largest value of this ratio measured to date in this laboratory. This large value for  $\sigma_i/\sigma_d$  indicates the strong dominance of defect accumulation in the amorphization process. At low doses ( $<0.3$  dpa), both amorphization and interstitial defects contribute to the relative disorder, which may explain why the relative disorder is slightly higher than that indicated by the model fit in this dose range.

### 3.2. DAMAGE RECOVERY

The specimens irradiated with 1.0 MeV  $\text{Au}^{2+}$  ions (Figure 1) were subsequently annealed at 300 K for 13 hours in order to investigate the amount of recovery for a given level of disorder. The amount of recovered disorder as a function of pre-existing, irradiation-induced disorder is shown in Figure 2 and should be proportional to the relative contribution of interstitial defects to the measured disorder. The results indicate that the maximum recovery probably occurs between 40% and 80% disorder, which is where the product of the crystalline fraction,  $1-f_a$ , and the concentration of irradiation-induced point defects in the residual crystalline phase reaches a maximum. The relative recovery at a pre-existing disorder of 1.0 decreases with dose, indicating some continued defect contribution to the disorder as it initially reaches the random level.

Single crystals of  $\text{SrTiO}_3$  were irradiated at 180 K to low doses with 410 keV  $\text{He}^+$  or 400 keV  $\text{O}^+$  to produce a partially damaged state ( $<25\%$  disorder at the damage peak) consisting primarily of point defects. The recovery of defects in these samples was studied by isochronal annealing. The recovery behavior for disorder on the oxygen sublattice at the damage peak is shown in Figure 3 for  $\text{SrTiO}_3$  irradiated with 400 keV

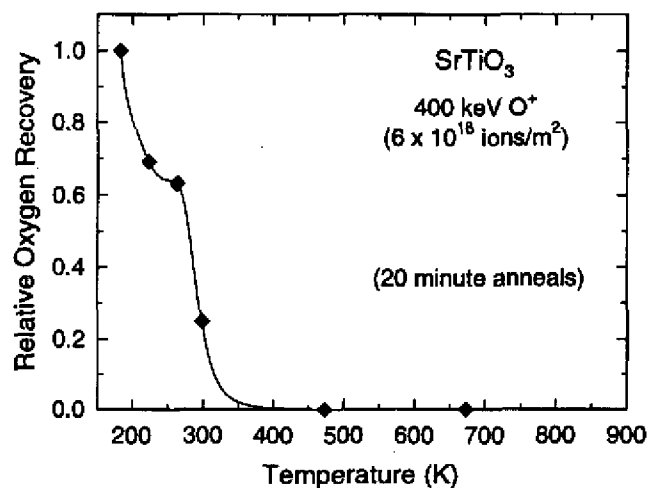


Figure 3. Isochronal recovery on the oxygen sublattice at the damage peak for  $\text{SrTiO}_3$  irradiated with 400 keV  $\text{O}^+$  ions at 180 K.

$\text{O}^+$  ions. The results indicate that thermal recovery processes on the oxygen sublattice are complete after annealing at 475 K for this sample and these irradiation conditions. The results also suggest the presence of two recovery stages on the oxygen sublattice, with peak recoveries at about 200 and 300 K, respectively. Based on experimental studies [13,14] the activation energy for migration of oxygen vacancies in single crystal  $\text{SrTiO}_3$  is on the order of 0.98 to 1.3 eV, and a computer simulation study of defects in  $\text{SrTiO}_3$  [15] indicates that the oxygen vacancy has a minimum migration energy of 0.65 eV. More recently, computer simulation studies at PNNL indicate that the minimum migration energy for the oxygen interstitial in  $\text{SrTiO}_3$  is about 0.2 eV, and further computer simulation studies are in progress. These activation energies for migration of point defects on the oxygen sublattice are consistent with the recovery behavior observed in Figure 3.

Thermal recovery of the disorder on the cation sublattice at the damage peak is shown in Figure 4 for  $\text{SrTiO}_3$  single crystals irradiated with either 410 keV  $\text{He}^+$  ions or 400 keV  $\text{O}^+$  ions. The results show a single recovery stage between 200 and 400 K, and gradual recovery at higher temperatures, which is similar to the recovery behavior previously observed in  $\text{SrTiO}_3$  irradiated with 1.0 MeV  $\text{Au}^{2+}$  [10] to low ion fluences. Complete recovery on the cation sublattice occurs at temperatures above 900 K. Based on computer simulations [15], the cation vacancy migration energies are 2.52 and 11.6 eV for Sr and Ti, respectively, which suggests these defects are relatively immobile during irradiation and thermal annealing. The results of preliminary computer simulations at PNNL indicate that long-range migration of Sr and Ti interstitials require activation energies of 4.34 and 3.33 eV, respectively; however, short-range migration pathways also exist for Sr and Ti interstitials with activation energies of 0.96 and 0.87 eV, respectively. Such short-range migrations would produce only partial recovery from the recombination of close-pairs, which is consistent with the behavior observed

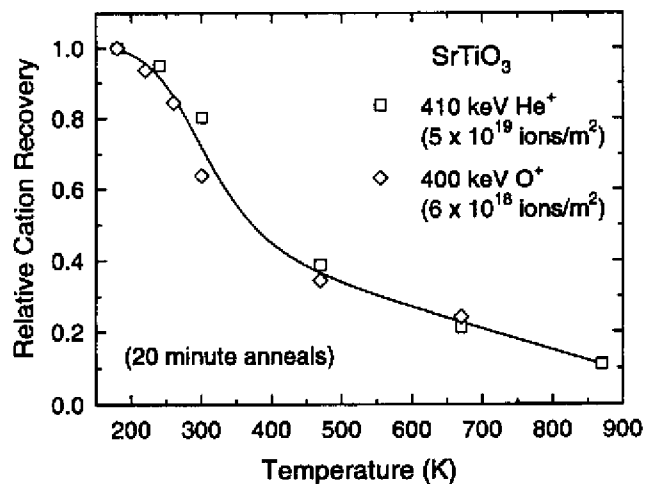


Figure 4. Isochronal recovery on the cation sublattice for  $\text{SrTiO}_3$  irradiated with 410 keV  $\text{He}^+$  or 400 keV  $\text{O}^+$  ions at 180 K.

in Figure 4. Furthermore, oxygen defects will induce minor displacements of neighboring cations, which will contribute somewhat to the observed disorder on the cation sublattice. Consequently, the recovery of defects on the oxygen sublattice should also relieve some local displacive disorder on the cation sublattice.

### 3.3. TEMPERATURE DEPENDENCE OF AMORPHIZATION

The temperature dependence of the dose necessary to achieve the amorphous state, as determined by TEM techniques, in  $\text{SrTiO}_3$ ,  $\text{CaTiO}_3$ , and  $\text{BaTiO}_3$  irradiated with 800 keV  $\text{Kr}^+$  ions has been reported previously [9], and the results are summarized in Figure 5. (Note: the dose in Figure 5 has been renormalized based on a displacement energy of 25 eV.) As discussed previously [9], the amorphization dose is not noticeably affected by the displacive phase transition at 108 K in  $\text{SrTiO}_3$ ; in the case of  $\text{BaTiO}_3$ , however, the displacive phase transition at 393 K results in a minor decrease in amorphization dose with increasing temperature. The critical temperature,  $T_c$ , above which the TEM-amorphous state cannot be produced under these irradiation conditions, increases from 425 K for  $\text{SrTiO}_3$  to 550 K for  $\text{BaTiO}_3$ . The critical temperatures are summarized in Table 1, along with the temperature,  $T_r$ , for thermal epitaxial recrystallization of amorphous layers in these materials [1,4,8,16]. If a thermal recovery process controls the critical temperature for amorphization, then  $T_c$  will generally exceed the temperature at which the thermal recovery process is normally active (in the absence of irradiation) because the rate of thermal recovery must balance the damage production rate [12]. It is clear that thermal epitaxy occurs at temperatures much higher than the critical temperature for amorphization. Consequently, processes other than thermal epitaxy should control the critical temperature for amorphization in these materials. In the case of  $\text{SrTiO}_3$ , the thermal defect recovery stages that are observed at 300 K for

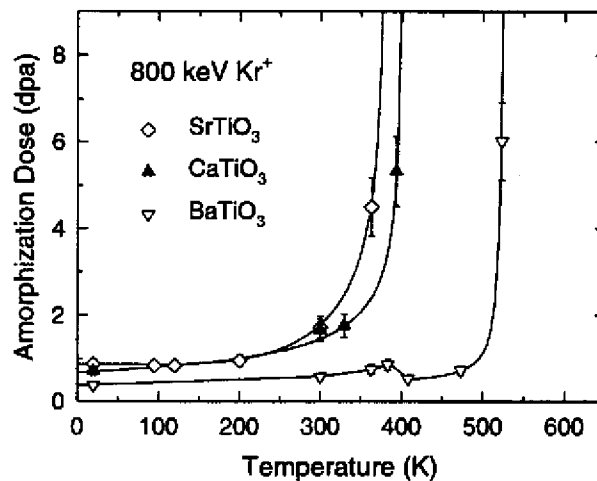


Figure 5. Temperature dependence of dose to reach TEM amorphous state in  $\text{SrTiO}_3$ ,  $\text{CaTiO}_3$ , and  $\text{BaTiO}_3$  irradiated with 800 keV  $\text{Kr}^+$  (adapted from Meldrum et al. [9])

anions and cations in Figures 3 and 4 could be the recovery processes controlling the critical temperature and inhibiting amorphization.

The dose necessary to achieve the TEM amorphous state in  $\text{SrTiO}_3$  irradiated with 800 keV  $\text{Kr}^+$  or 800 keV  $\text{Xe}^+$  ions is shown in Figure 6 as a function of temperature. The amorphization dose in  $\text{SrTiO}_3$  is relatively independent of irradiation temperature below 200 K. Above this temperature, the amorphization dose increases with temperature. This onset for an observable effect of temperature on amorphization is consistent with the onset of thermal defect recovery processes in Figures 3 and 4. The temperature dependence of the amorphization dose shows only a weak dependence on the damage-energy density (i.e., ion mass) for these ions and is mostly within experimental error. The critical temperature under  $\text{Kr}^+$  irradiation may be slightly lower (<20 K) than under  $\text{Xe}^+$  irradiation, and this is consistent with a slightly lower damage production rate for  $\text{Kr}^+$  relative to  $\text{Xe}^+$ . The weak dependence of  $T_c$  on damage-energy density in Figure 6 is consistent with the critical temperature being controlled by a

TABLE 1. Critical temperature,  $T_c$ , for amorphization under irradiation with 800 keV  $\text{Kr}^+$  ions [9] and the temperature,  $T_r$ , for epitaxial recrystallization.

Material	$T_c$ (K)	$T_r$ (K)
$\text{SrTiO}_3$	425	575 [1,4]
$\text{CaTiO}_3$	440	685 [8]
$\text{BaTiO}_3$	550	<1375 [16]

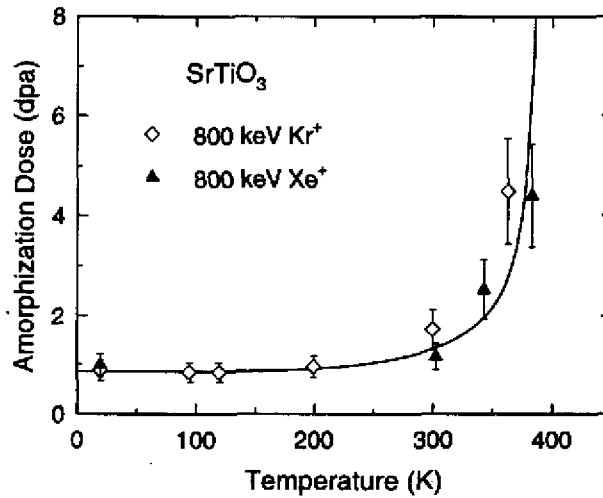


Figure 6. Temperature dependence of dose to reach the TEM amorphous state in  $\text{SrTiO}_3$  irradiated with 800 keV  $\text{Kr}^+$  or 800 keV  $\text{Xe}^+$  ions.

thermal recovery process, as described previously [12]. However, irradiation with lighter ions (lower energy density) may exhibit a decrease in  $T_c$  as irradiation-assisted recovery processes become dominant [12].

A relationship between dose and temperature to achieve a specific amorphous state has been recently derived based on the kinetic direct-impact/defect-stimulated model for amorphization [12], which considers both epitaxial recrystallization,  $K_r(T)$ , and defect recombination/annihilation,  $K_d(T)$ , rates. Since epitaxial recrystallization does not appear to play a significant role in the temperature dependence of amorphization in  $\text{SrTiO}_3$ , the dose to achieve a specific amorphous state in this material is given by the expression [12]:

$$D = [D_0 + A\phi \ln\{1 - AK_d(T)[1 - \exp(-D_0/\phi A)]\}] / [1 - AK_d(T)], \quad (2)$$

where  $A = [\phi (\sigma_a + \sigma_s)]^{-1}$ ,  $\phi$  is the ion flux, and  $D_0$  is the dose to achieve the specific amorphous state at 0 K. Furthermore, as noted elsewhere [12], the recovery rate in Eq. (2) is the sum of temperature-dependent rate constants for both irradiation-assisted and thermal annealing processes (i.e.,  $K_d(T) = K_{ir}(T) + K_{th}(T)$ ), each with its own effective jump frequency and activation energy. The irradiation-assisted recovery processes may be nearly athermal with low activation energies. The result of an iterative fit of Eq. (2) to the data is shown in Figure 6 and yields activation energies of  $0.1 \pm 0.05$  eV and  $0.6 \pm 0.1$  eV for irradiation-assisted and thermal recovery processes, respectively. The activation energy of  $0.6 \pm 0.1$  eV for the thermal recovery process is consistent with the thermal recovery processes in Figures 3 and 4 and with the calculated activation energy for oxygen vacancy migration [15].

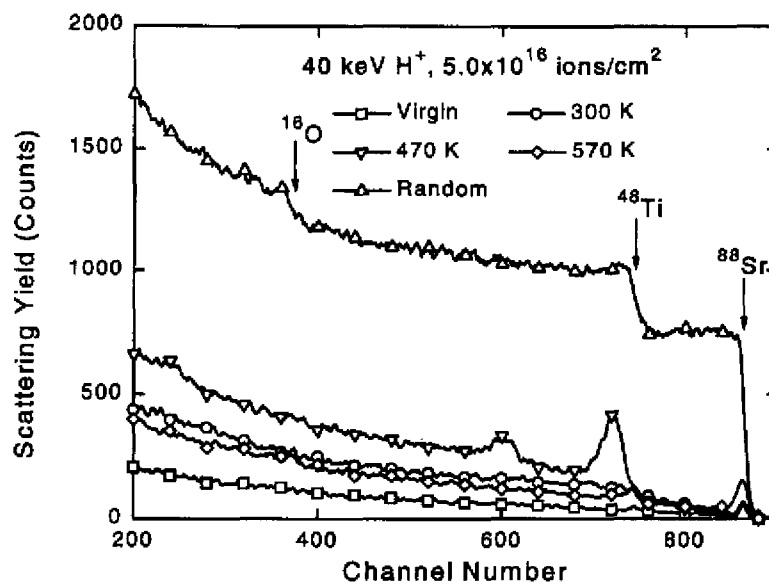


Figure 7. RBS/C backscattering spectra from  $\text{SrTiO}_3$  after hydrogen implantation to  $5.0 \times 10^{16} \text{ ions/cm}^2$  and after isochronal annealing.

### 3.4. EFFECTS OF HYDROGEN IMPLANTATION

The channeling spectra from the irradiated and virgin regions are presented as a function of annealing temperature, along with the random spectrum, in Figure 7 for an ion fluence of  $5.0 \times 10^{16} \text{ H}^+/\text{cm}^2$ . Only the RBS/C spectra from the irradiated region after isochronal annealing at 300, 470 and 570 K are shown to minimize the overlap of different spectra. As expected, the irradiation-induced disorder (300 K spectrum) on both the Ti and Sr sublattices is rather dilute. The as-implanted hydrogen concentration profile and several profiles after annealing are shown in Figure 8. The as-implanted hydrogen concentration profile (300 K) shows a broad profile due to diffusion and a maximum at about 300 nm, which according to TRIM calculations is where the peak of the implanted hydrogen profile should occur. The measurements indicate that the total amount of hydrogen within the analyzed region is  $4.43 \times 10^{16} \text{ H/cm}^2$ , which indicates that some hydrogen has diffused to the surface or beyond the analyzed region. Annealing the sample to 370 K resulted in a slight increase in the backscattering yield from the Sr and Ti sublattices (not shown) suggesting that there is some increased disordering due to annealing, perhaps as a result of hydrogen coalescence. The maximum in the hydrogen profile after annealing at 370 K shifts to a depth of 275 nm, which is coincident with the damage peak predicted by TRIM. Furthermore, the hydrogen profile sharpens somewhat after annealing at 370 K, and the total amount of hydrogen in the analyzed region is reduced slightly to  $4.26 \times 10^{16} \text{ H/cm}^2$ .

The local disorder generated on the Sr and Ti sublattices is significantly increased near the damaged peak position after annealing at 470 K (Figure 7). The local disorder

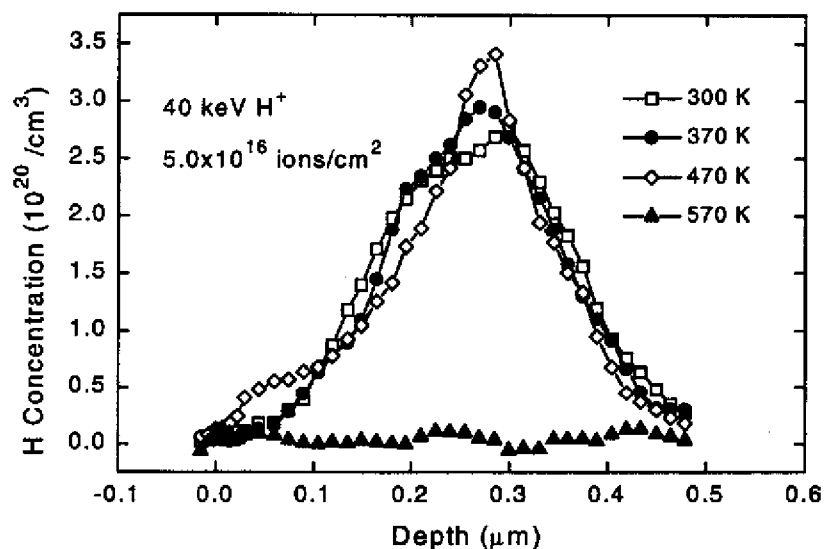


Figure 8. Hydrogen profile, based on nuclear reaction analysis, in  $\text{SrTiO}_3$  after hydrogen implantation to  $5.0 \times 10^{16} \text{ ions/cm}^2$  and after isochronal annealing.

on these two sublattices is well separated in the spectrum and is very prominent compared to the disorder generated from implantation damage. The total amount of hydrogen after annealing at 470 K remains unchanged ( $4.26 \times 10^{16} \text{ H/cm}^2$ ). The hydrogen profile indicates some diffusion towards the surface; however, the peak in the profile at 275 nm becomes more pronounced. Since scanning electron microscopy (SEM) results indicate the presence of hydrogen blisters at higher annealing temperatures [11], the increase in backscattering yield at the damage peak is believed to be caused by the nucleation of  $\text{H}_2$  bubbles, which locally distort the structure and provide new scattering surfaces. The shift in the peak of the hydrogen profile to coincidence with the peak in the damage profile indicates diffusion and trapping of the hydrogen at irradiation-induced defects. Annealing at 570 K results in a significant decrease in the RBS/C backscattering yield from the peak damage region, an increase in the backscattering yield from the surface peak region, and a slight increase in the backscattering from the region between the surface peak and the damage peak. The hydrogen profile after annealing at 570 K indicates a significant loss of hydrogen from the implanted region. SEM results indicate that large cleaved areas exist after annealing this sample. This behavior is similar to the so-called "smart cutting" observed in Si [17], which suggests that it may be possible to produce large cleaved single crystals of titanate perovskites with a controlled thickness on the order of 50 nm to several hundred nanometers for research or device applications.

Similar RBS/C and hydrogen profiles have been obtained for an ion fluence of  $1.0 \times 10^{17} \text{ H}^+/\text{cm}^2$ . In these samples, annealing at 570 K results in a much larger increase in the RBS/C backscattering yield across the penetration depth of the implanted hydrogen. The hydrogen profile after annealing at 570 K indicates an increase in the hydrogen

concentration near the surface region and a decrease in the total amount of hydrogen within the analyzed region, but not a complete loss of hydrogen as observed for  $5.0 \times 10^{16} \text{ H}^+/\text{cm}^2$ . The sudden increase in the backscattering yield across the penetration depth is caused by the deformation of the surface region due to the formation of large hydrogen blisters, which are large enough to misorient the blister surface relative to the substrate. Annealing at 670 K reduces the total amount of hydrogen, as the blisters begin to burst, and after annealing at 770 K, the hydrogen is nearly completely lost. This behavior is due to the blisters bursting and releasing  $\text{H}_2$  gas, which leads to both exfoliated blister surfaces and blister caps, as shown by SEM [11].

#### 4. Conclusions

Ion-beam irradiation of  $\text{SrTiO}_3$ ,  $\text{CaTiO}_3$ , and  $\text{BaTiO}_3$  results in a crystalline-to-amorphous transformation below a critical temperature. In the case of irradiation with 800 keV  $\text{Kr}^+$  ions, this critical temperature is 425, 440 and 550 K for  $\text{SrTiO}_3$ ,  $\text{CaTiO}_3$  and  $\text{BaTiO}_3$ , respectively. Ion-channeling studies of damage accumulation in  $\text{SrTiO}_3$  irradiated with 1.0 MeV  $\text{Au}^{2+}$  ions suggest that the crystalline-to-amorphous transformation is dominated by the accumulation and interaction of irradiation-induced defects. In  $\text{SrTiO}_3$  irradiated with  $\text{He}^+$  and  $\text{O}^+$  ions at 180 K, isochronal annealing studies indicate that there is significant recovery of defects on both the oxygen and cation sublattices between 200 and 400 K. These defect recovery processes may control the kinetics of amorphization. A fit of the direct-impact/defect-stimulated model to the data for  $\text{SrTiO}_3$  suggests that the kinetics of amorphization are controlled by both a nearly athermal irradiation-assisted recovery process with an activation energy of  $0.1 \pm 0.05$  eV and a thermal defect recovery process with an activation energy of  $0.6 \pm 0.1$  eV. In  $\text{SrTiO}_3$  implanted with 40 keV  $\text{H}^+$ , annealing at 470 K results in increased backscattering from Sr and Ti in the damage peak due to the nucleation of  $\text{H}_2$  bubbles; annealing at 570 K and higher results in the formation of blisters or large cleaved areas.

#### Acknowledgements

This research was sponsored by the US Department of Energy through the Division of Materials Sciences, Office of Basic Energy Sciences and the Environmental Management Science Program at both PNNL and ORNL. The work at PNNL was performed under Contract DE-AC06-76RLO 1830, and the work at ORNL was performed under Contract DE-AAC05-96OR. AM also acknowledges support from NSERC, Canada. This study utilized the accelerator facilities within the Environmental Molecular Sciences Laboratory at PNNL, which is a national scientific user facility sponsored by the DOE Office of Biological and Environmental Research. The authors also gratefully acknowledge the staff at the HVEM-Tandem facility (ANL) for assistance with the irradiation experiments.

## References

1. White, C.W., Boatner, L.A., Sklad, P.S., McHargue, C.J., Rankin, J., Farlow, G.C., and Aziz, M.J. (1988) Ion implantation and annealing of crystalline oxides and ceramic materials, *Nucl. Instrum. and Methods B* **32**, 11-22.
2. White, C.W., McHargue, C.J., Sklad, P.S., Boatner, L.A., and Farlow, G.C. (1989) Ion implantation and annealing of crystalline oxides, *Material Science Reports* **4**, 41-146.
3. McCallum, J.C., Rankin, J., White, C.W., and Boatner, L.A. (1990) Time resolved reflectivity measurements in Pb-implanted SrTiO<sub>3</sub>, *Nucl. Instrum. and Methods B* **46**, 98-101.
4. Rankin, J., McCallum, J.C., and Boatner, L.A. (1992) The effect of annealing environments on the epitaxial recrystallization of ion-beam-amorphized SrTiO<sub>3</sub>, *J. Materials Research* **7**, 717-724.
5. Simpson, T.W., Mitchell, I.V., McCallum, J.C., and Boatner, L.A. (1994) Hydrogen catalyzed crystallization of strontium titanate, *J. Applied Physics* **76**, 2711-2718.
6. Rankin, J., Sheldon, B.W., and Boatner, L.A. (1994) The measurement and analysis of epitaxial recrystallization kinetics in ion-beam-amorphized SrTiO<sub>3</sub>, *J. Materials Research* **9**, 3113-3120.
7. Overwijk, M.H.F., Cillessen, J.F.M., Kessener, Y.A.R.R., and Tenner, M.G. (1994) Incorporation of Nd in pulsed-laser-deposited compared to ion-implanted SrTiO<sub>3</sub>, *Nucl. Instrum. and Methods B* **91**, 322-326.
8. Rankin, J., McCallum, J.C., and Boatner, L.A. (1995) Annealing environment effects in the epitaxial regrowth of ion-beam-amorphized layers on CaTiO<sub>3</sub>, *J. Applied Physics* **73**, 1519-1527.
9. Meldrum, A., Boatner, L.A., and Ewing, R.C. (1998) Effects of ionizing and displacive irradiation on several perovskite-structure oxides, *Nucl. Instrum. and Methods B* **141**, 347-352.
10. Thevuthasan, S., Jiang, W., Weber, W.J., and McCready, D.E. (1999) Damage accumulation and thermal recovery in SrTiO<sub>3</sub> implanted with Au<sup>2+</sup> ions, in S.J. Zinkle, G.E. Lucas, R.C. Ewing, and J.S. Williams (eds.), *Microstructural Processes in Irradiated Materials*, Mater. Res. Soc. Symp. Proc. **540**, Warrendale, PA, pp. 373-378.
11. Thevuthasan, S., Jiang, W., Young, J.S., and Weber, W.J. (1999) Investigation of thermal recovery behavior in hydrogen-implanted SrTiO<sub>3</sub> using high energy ion beam techniques, *Nucl. Instrum. and Methods*, in press.
12. Weber, W.J. (1999) Models and mechanisms of irradiation-induced amorphization in ceramics, *Nucl. Instrum. and Methods*, in press.
13. Yamaji, A. (1975) Oxygen-ion diffusion in single-crystal and polycrystalline SrTiO<sub>3</sub>, *J. Amer. Ceram. Society* **58**, 152-153.
14. Paladino, A.E., Rubin, L.G., and Waugh, J.S. (1965) Oxygen ion diffusion in single crystal SrTiO<sub>3</sub>, *J. Phys. Chem. Solids* **26**, 391-397.
15. Akhtar, M.J., Aakhtar, Z.-U.-N., Jackson, R.A., and Catlow, C.R.A. (1995) Computer simulation studies of strontium titanate, *J. Amer. Ceramic Society* **78**, 421-428.
16. Gea, L., Honda, S., Boatner, L.A., Haynes, T.E., Sales, B.C., Modine, F.A., Meldrum, A., Budai, J.D., and Beckers, L. (1998) A new approach to the fabrication of "smart" near-surface nanostructure composites, in K.E. Gonsalves, M.I. Baraton, R. Singh, H. Hofmann, J.X. Chen, J.A. Akkara (eds.), *Surface-Controlled Nanoscale Materials for High-Added-Value Application*, Mater. Res. Soc. Symp. Proc. **501**, Warrendale, PA, pp. 137-142.
17. Breese, M.B.H., de Kerckhove, D.G., Hoechbauer, T., and Nastasi, M. (1999) Analysis of the crystalline quality and hydrogen content in "smart cut" silicon, *Nucl. Instrum. and Methods*, in press.